JOURNAL OF SOLID STATE CHEMISTRY 1, 28–38 (1969)

Multiple Phase Formation in the Binary System Nb_2O_5–WO_3

VII. Intergrowth of H–Nb_2O_5 and $WNb_{12}O_{33}$

J. G. ALLPRESS† AND A. D. WADSLEY‡

Received December 27, 1968

A number of high-temperature mixed oxides of niobium and tungsten, containing less than 10 mole percent WO_3, have been examined by electron diffraction and microscopy. The unit cell dimensions and symmetries of three new phases found in this region have been determined. The structures proposed for them are based upon the ordered intergrowth of high temperature Nb_2O_5 and $WNb_{12}O_{33}$, leading to the ideal compositions $WNb_{26}O_{68}$, $WNb_{40}O_{103}$ and $WNb_{68}O_{173}$. Lattice images of suitably oriented fragments of these materials proved to be particularly useful in elucidating the structural relationships between them. The observations pose a number of questions concerning definitions in solid state chemistry.

Introduction

Parts I–V of this continuing study concerned the X-ray identification and crystal structure analyses of five phases found in the Nb_2O_5–WO_3 system (*1–5*). The structure of each one consisted of rectilinear blocks of corner-shared octahedra, joined through common edges at shear planes, and with tetrahedrally coordinated metals at the centres of the junctions between any four blocks. All of these mixed niobium–tungsten oxides may have small but finite ranges of homogeneity. A fully-refined structure determination, however, is based upon an ideal formula, and the crystalline imperfections associated with any variation of composition are disregarded in these diffraction studies.

There is still some uncertainty in the identity of a number of suspected phases close in composition to Nb_2O_5. Roth and Wadsley (*1*) in Part I found X-ray evidence for a compound near $WO_3 \cdot 15Nb_2O_5$, and Gruehn (*6*), without giving any details, reported a phase with a range of homogeneity within the composition limits $WO_3 \cdot 20Nb_2O_5$–$WO_3 \cdot 40Nb_2O_5$. Roth and Waring (*7*) also described a compound close to $WO_3 \cdot 30Nb_2O_5$, which might well be identical with Gruehn's material.

The problem of characterizing a new phase in this particular area of solid state chemistry, especially when it is nonstoichiometric, depends in the first instance upon the assignment of its unit cell. When this is large and oblique, an X-ray examination of an untwinned single crystal is the conventional way of providing an unambiguous answer, and definitive X-ray studies are therefore limited in practice to those cases where crystals large enough to be manipulated have been grown. Thereafter the crystal structure determination is facilitated by a number of useful working rules. The presence of the rectilinear blocks—which have the ReO_3 structure—invariably gives a prominent cubic subcell, from which the orientation of the blocks relative to the unit cell are determined. The symmetry and space group have their obvious importance, and the contents of the unit cell are required to match the composition of the phase within very close limits, although there are obvious difficulties when this is variable. With these criteria in mind, the idealized arrangement of octahedral blocks with their tetrahedral interstices can usually be found readily enough, and the more formal approach to the structure via the Patterson function is a standby for the occasion when a new or unforseen principle emerges.

The X-ray method, however, becomes progressively more difficult to apply as the size of the unit cell increases. Very small crystals are usually all that are available for data collection, many of the weak superlattice reflexions are not recorded, and it can be a difficult and frustrating problem even to determine the crystallographic constants unambiguously. In addition, the number of independent

† Division of Tribophysics, CSIRO, University of Melbourne, Australia.

‡ Deceased January 6, 1969. Division of Mineral Chemistry, CSIRO, Melbourne, Australia.

parameters needed to describe the structure may become comparable with the number of available data, thus precluding a satisfactory refinement.

Some of these difficulties can be overcome with electron optical techniques. Provided that a suitable, thin crystal can be tilted into the appropriate position, electron diffraction patterns of simple orientations can be obtained. It is quite easy to record all of the data within a particular zone with an exposure of less than 1 min. The diffraction pattern corresponds to a section through the reciprocal lattice, and the determination of the unit cell from several of these sections is straightforward. Moreover, lattice images of the crystals can be observed (*8*). We have shown in Part VI of this series (*9*) that these images contain detailed information of the faulting in the Nb–W mixed oxides, and that the faults afford a means of accommodating small ranges of composition.

In the present paper, we describe the application of these electron optical techniques to the mixed Nb–W oxides containing less than 10 mole percent WO_3, in an effort to elucidate the compositions and structures of the phases which might be present. We have not attempted to make use of the electron diffraction intensity data to derive the atomic positions, but instead have limited ourselves to proposing idealized structures which are geometrically consistent with the observed data. This approach may be justified because of the confidence with which unit cell dimensions can be predicted in this system (*9*), and there is little to be gained by the forbidding amount of additional labor which would be involved in making a rigorous determination.

Experimental

Most of the samples of the mixed oxides of Nb and W were taken from batches prepared for the phase study described in Part I of this series (*1*). Their nominal compositions were Nb_2O_5:WO_3 = 11:1, 13:1, 15:1, 30:1. Additional samples with compositions 40:1 and 60:1 were kindly provided by Dr. R. Gruehn, University of Münster, Westphalia.

Techniques for preparing specimens for the electron microscope and their subsequent examination have already been described (*8*, *9*). In some cases, a thin layer of aluminium was deposited on the microscope grids bearing the oxide samples to calibrate electron diffraction patterns.

Results

Electron Diffraction

All the samples were mixtures of several compounds, and even individual crystal fragments sometimes contained more than one phase. The electron diffraction patterns indicated that these compounds were all closely related. They were all monoclinic with a short unique axis, *b*, of about 3.8 Å, in common with most of the high-temperature mixed oxides and oxyfluorides of niobium (*10*). When suitable crystals were tilted so that the incident electron beam was parallel to this short axis, a total of five different *h*0*l* diffraction patterns could be distinguished, including those of H–Nb_2O_5 and

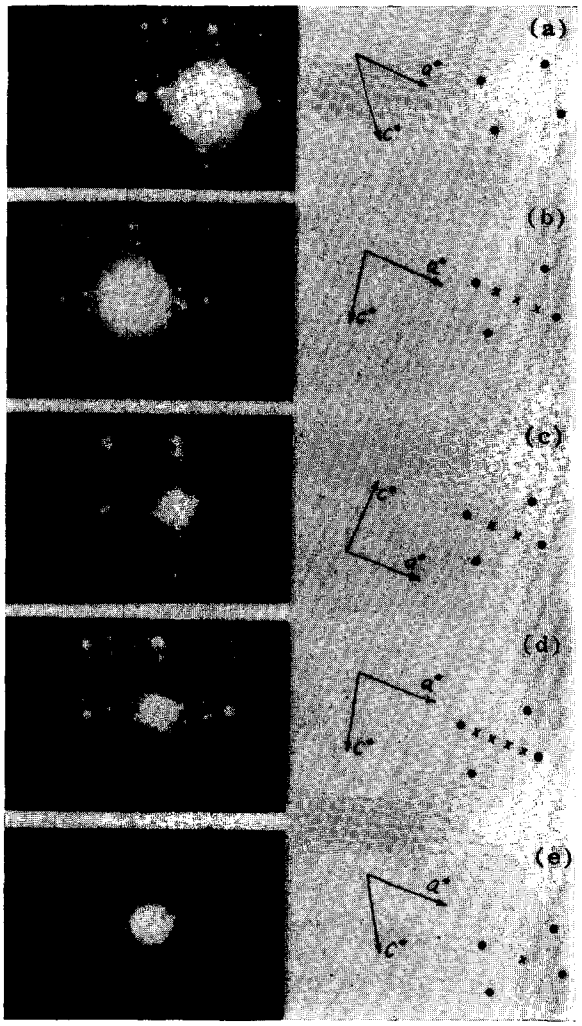

FIG. 1. Electron diffraction patterns. *h*0*l* sections of the reciprocal lattices of the phases found in the composition region between Nb_2O_5 and $WNb_{12}O_{33}$. A small enlarged area of each pattern is sketched alongside it, showing the subdivision of the reciprocal axis, a^*. 1a. $WNb_{12}O_{33}$; 1b. The new phase $WNb_{26}O_{68}$; 1c. The new phase $WNb_{40}O_{103}$; 1d. A combination of $WNb_{40}O_{103}$ and the third phase $WNb_{68}O_{173}$ where a^* is subdivided by 5; 1e. H–Nb_2O_5.

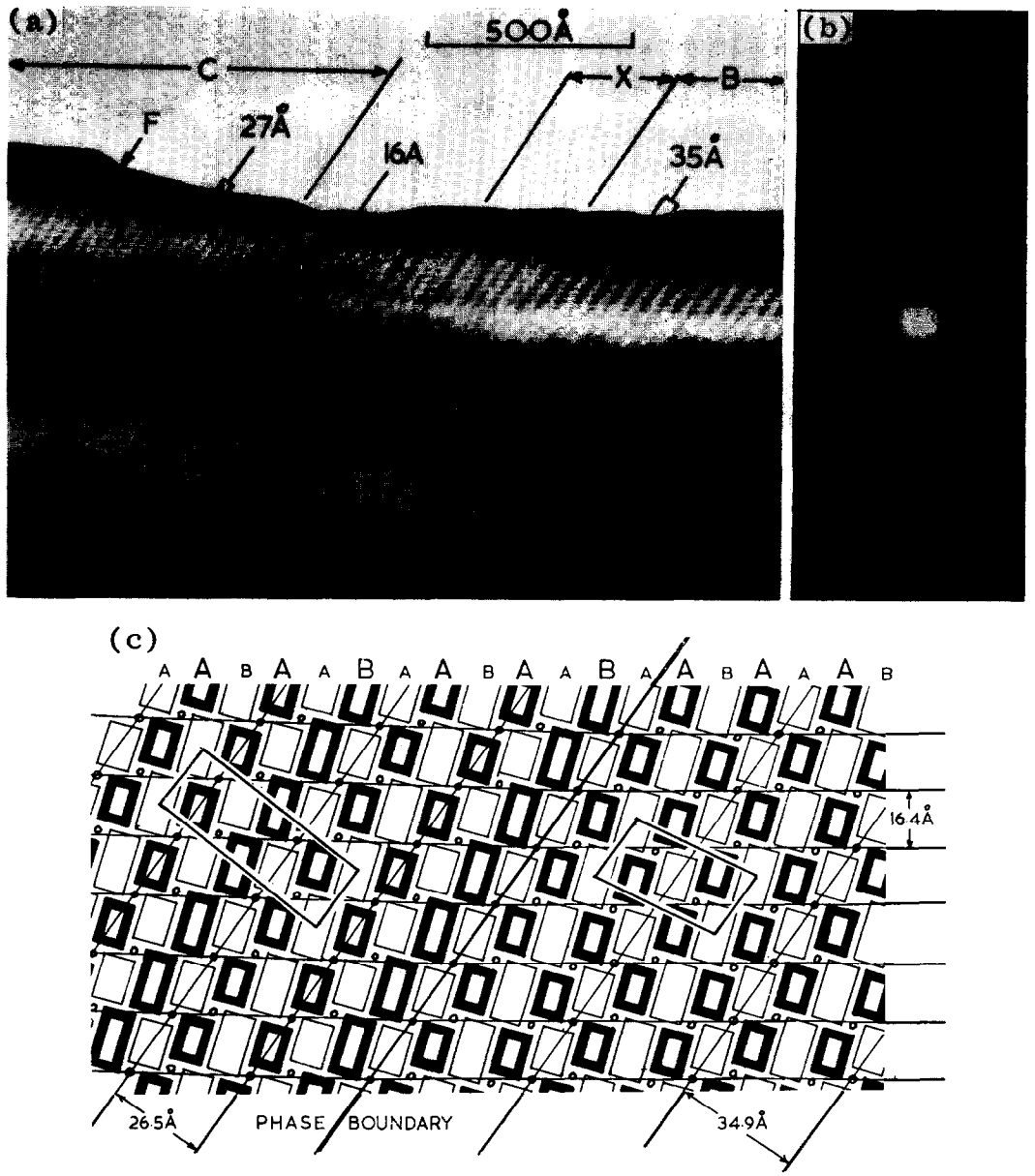

FIG. 2a. Lattice image of a crystal fragment with domains of $WNb_{26}O_{68}$ at B, and $WNb_{40}O_{103}$ at C, separated by a faulted region containing a microdomain X with a different fringe sequence. F is a single fault. 2b. Electron diffraction pattern of the crystal fragment in Fig. 2a. 2c. Idealized model of the region enclosed by the rectangle in Fig. 2a. The rectangles in darker and lighter outline correspond to blocks of octahedra centered at two levels, the circles being tetrahedral atoms. The phase boundary separates domains of $WNb_{26}O_{68}$ (right) from $WNb_{40}O_{103}$ (left). The rows of blocks are labelled according to the text, and the calculated fringe spacings are given. The unit cells of the two phases are outlined.

$WNb_{12}O_{33}$ (Fig. 1). $WNb_{12}O_{33}$ was the simplest of these, and the others were all related to it by a subdivision of the reciprocal-lattice unit-cell edge marked a^* in Fig. 1a. This axis is halved in H–Nb_2O_5 (e), and divided by 3 in (c) and 4 in (b). The pattern in (d) can be resolved into two simpler ones in which these factors are 3 (as in (c)) and 5. The pattern (c) was most frequently observed, (b) was found only together with (a) and (c) in the mixtures richer in WO_3 (11:1–15:1) while (d) was seen only rarely in the 60:1 mixture, along with (c) and (e). Hence it seemed likely that the proportion of WO_3 in each

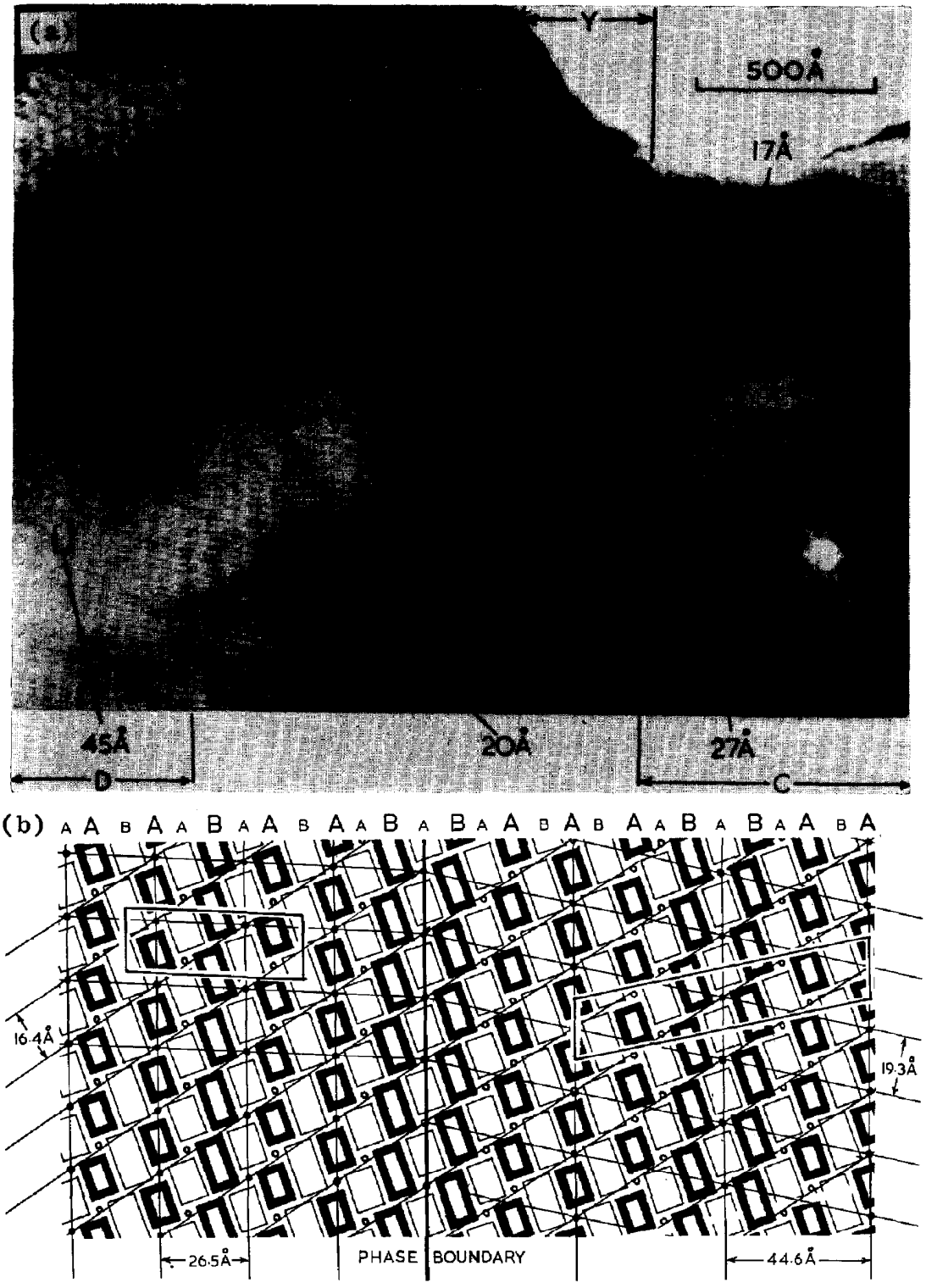

FIG. 3a. Lattice image of a crystal fragment with domains of $WNb_{40}O_{103}$ at C and $WNb_{68}O_{173}$ at D separated by a faulted region. Y is the different fringe sequence discussed in the text. The diffraction pattern of the fragment is inset. 3b. Idealized model of the region enclosed in the rectangle in Fig. 3a.

of the three new phases followed the order (b) > (c) > (d).

Other sections through the reciprocal lattices must be obtained in order to determine the additional symmetry elements of the phases. The simplest method of examining H–Nb_2O_5 and $WNb_{12}O_{33}$ was to record the *hk*0 and 0*kl* patterns from crystals of pure samples. On the other hand the new phases were always associated with others in any one sample, and to obtain unambiguous evidence to supplement the *h*0*l* sections it was necessary to record other sections from the same crystal fragment. Crystals were tilted about their a^* axes through angles of up to 50°, the maximum angle available in the electron microscope specimen holder, to record layer lines containing reflections with indices *h n nm*, where *m* is constant and $n = 1, 2, 3 \ldots$. Typically these were the *h*00, *h*16, *h*2 12, *h*3 18 .... reflections, which were examined for systematic absences characteristic of centering or of glide planes.

Side centering was demonstrated for $WNb_{12}O_{33}$, in accordance with its known structure, as well as for the two cases shown in Figs. 1c and 1d, where the superlattices were derived from $WNb_{12}O_{33}$ by dividing a^* by an *odd* number. Primitive symmetry was found for H–Nb_2O_5 (Fig. 1e) and for the one additional diffraction pattern where a^* for $WNb_{12}O_{33}$ was divided by an *even* number (Fig. 1b). The unit cell dimensions in Table I were obtained from these electron diffraction data. The axial setting for $WNb_{12}O_{33}$ differs from the one given by Roth and Wadsley (*2*) but was chosen in order to emphasize the similarities between the five phases.

Transmission Electron Microscopy

Additional structural information was obtained from lattice images of suitably oriented thin crystals, recorded at maximum magnification (150,000×) using an objective aperture 25 μ in diameter. In addition to the direct electron beam, this aperture is able to pass diffracted beams with interplanar spacings, d_{hkl}, greater than about 10 Å, and results in the production of fringe contrast in the images, which are readily resolved. Ideally it would be expected that crystals oriented with their short *b* axes parallel to the beam would give the most informative images, because under these conditions there is a minimum overlap of atoms in the structures. In practice, however, the transmitted intensity was generally very low, and most of the images were recorded after tilting the crystals a few degrees away from this position to give diffraction patterns similar to that in Fig. 2b. The fringe spacings characterize a particular phase, and the changes in their direction across a phase boundary can be exploited to give valuable structural information.

Figures 2a and 3 are micrographs of regions where several different intersecting sets of fringes appear, and which therefore contain more than one phase. Two homogeneous regions marked B and C can be distinguished in Fig. 2a. The horizontal fringes with a regular spacing of 16 Å intersect the 27 Å fringes in the Area C at an angle of 58°, and the 35 Å fringes in B at 56°. The broad bands of light and dark contrast running parallel to the edge of the crystal are extinction fringes. These arise when the crystal is wedge-shaped, and when its thickness increases to several extinction distances for one or more of the intense reflexions in the diffraction pattern (Fig. 2b). The vertical fringes in Fig. 3 have a spacing of 27 Å in the Region C and 45 Å in D, while the area between them contains many faults. The horizontal 20 Å fringes intersect the regular fringes in C at an angle of 87°, and 78° in D. They deviate as they cross the faulted region. A third set with a period of 17 Å are also visible, and are inclined at 55 and 58° to the vertical fringes at C and D, respectively .

Interpretation

The very close relationships between the diffraction patterns of this group of five phases (Fig. 1) suggested to us that the three new compounds might well be ordered intergrowths, or hybrids, of the two end members H–Nb_2O_5 and $WNb_{12}O_{33}$, the idealised structures of which are drawn schematically in Figs. 4a and c. These structures contain *rows* of blocks of two kinds.

1. A Rows (Fig. 4b) containing blocks of octahedra four long and three wide joined by corners, and separated within the rows by metal atoms in tetrahedral coordination.

2. B Rows (Fig. 4d), where blocks of octahedra five long and three wide share edges within the rows.

In any unit cell the rows occur at two levels we will designate A and **A**, or B and **B**, normal to the axis of symmetry and separated by 1.9 Å (*b*/2), and are joined side by side through common octahedral edges.

$WNb_{12}O_{33}$ can be represented as the row sequence

—A—A—A—A—

and H–Nb_2O_5 by

—A—B—A—B—A—

H–Nb_2O_5 may be regarded as the simplest possible intergrowth between —A—A—A—A—, with the stoichiometry $M_{13}O_{33}$, and another structure

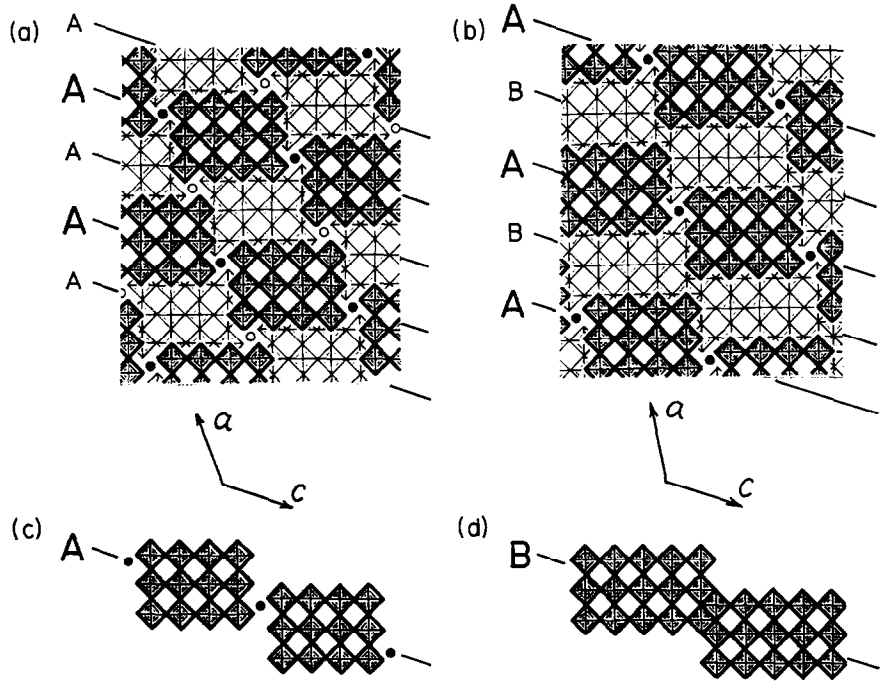

FIG. 4. The structures of $WNb_{12}O_{33}$ (4a) and H–Nb_2O_5 (4b) shown as sequences of the row components A (4c) and B (4d). These are cross-sections through the structures normal to the short (3.8 Å) axes of symmetry. Each square represents an octahedron viewed down a body diagonal, the darker squares within the rows A and B, and the lighter, within the Rows A and B, being centered on two parallel planes 1.9 Å apart. The octahedra sharing corners in any one of these planes form the structural blocks, and the junctions between light and dark lie in the shear planes. The circles are the tetrahedrally coordinated atoms located in the A and A Rows.

represented by —B—B—B—B— having the composition $M_{15}O_{37}$. This latter structure was predicted by one of us some time ago (*11*) and has recently been found for the compound $MgNb_{14}O_{35}F_2$ (*12*).

Since all three of the new Nb/W mixed oxides have *c* axes identical with each other, as well as with the two end members, they also probably contain ordered arrangements of A and B Rows, but with the condition that the ratio of the number of B Rows to A is less than one. The next simplest whole-number ratios B/A are 1/3, 1/2, and 2/3, and the corresponding row sequences are set out in Table II, together with the ratios 0 (for $WNb_{12}O_{33}$) and 1 ($Nb_{28}O_{70} = Nb_2O_5$), where the repeat distances, included in the braces, represent the extension of the unit cell. Note that these contain the symmetry, whether primitive or side-centered. The ideal composition of each phase can be deduced from the relative numbers of A and B Rows; for example, the ratio 1/3 has the combination of 3A and 1B, and the unit cell contains $3(M_{13}O_{33}) + 1(M_{15}O_{37})$, equal to $2(M_{27}O_{68})$. The composition can also be obtained, more laboriously but equally well, by counting atoms within the complete structures, which are shown in idealized form in Fig. 5. The theoretical unit cell dimensions can be estimated from these drawings by assuming a constant average octahedral edge of length 2.89 Å, and these are given in Table I for comparison with the measured electron diffraction values. We have shown previously (*9*) that such estimates are within ±2% of the data determined by X-rays for other members of this family of phases.

The fringe patterns of the lattice images provide additional evidence to corroborate these proposed structures. We will use a simplified representation of these structures where the individual blocks of octahedra are drawn as rectangles, the corners of which correspond to the corner metal atoms in the block (*9*). The diagram in Fig. 2c illustrates the coherent boundary between the two phases $WNb_{26}O_{68}$ and $WNb_{40}O_{103}$. Examples of this boundary appear in the micrograph in Fig. 2a, where the Region B is $WNb_{26}O_{68}$ and C is $WNb_{40}O_{103}$. The long axis fringe spacings calculated for these phases are 34.9 and 26.5 Å, respectively, and agree well with the observed spacings of 35 Å in B and 27 Å in C. The 16 Å fringes in Fig. 2a

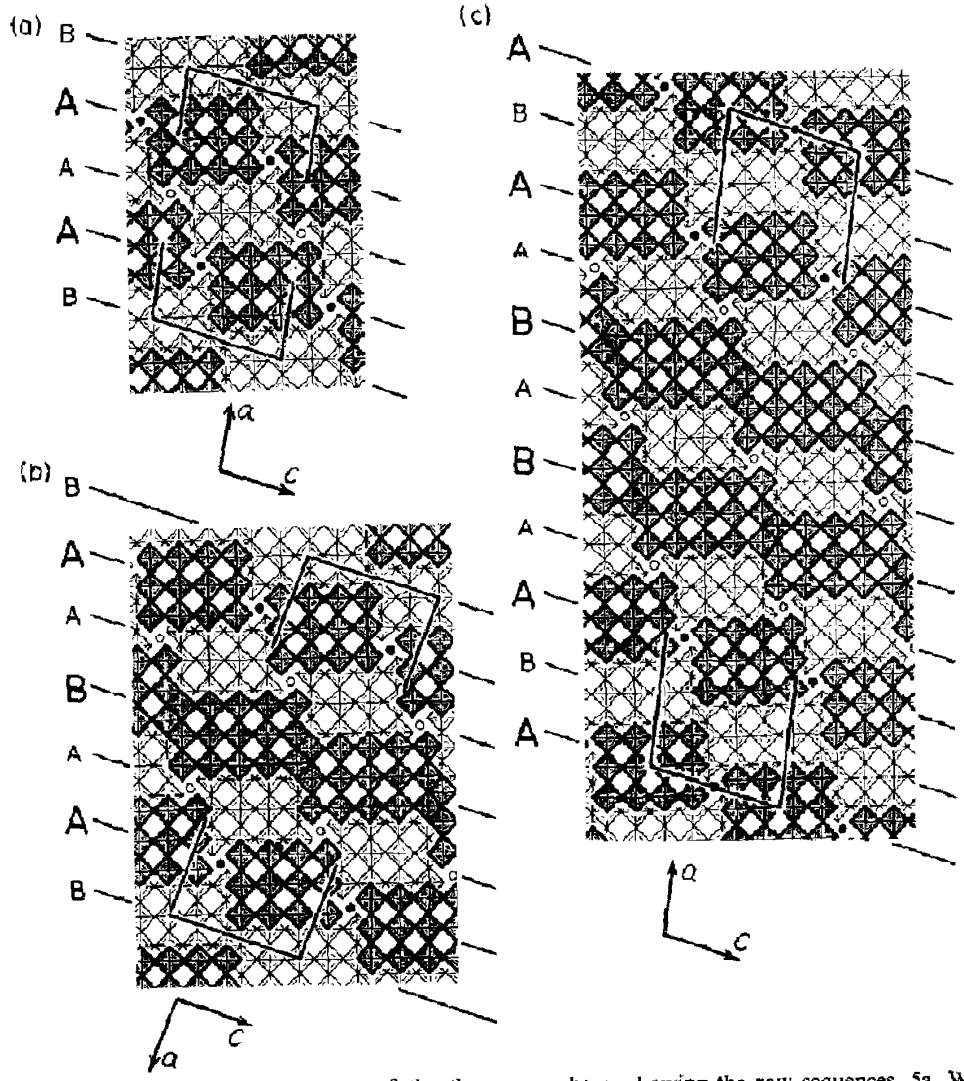

FIG. 5. Idealized models of the structures of the three new phases showing the row sequences. 5a. $WNb_{76}O_{88}$; 5b. $WNb_{40}O_{103}$; 5c. $WNb_{68}O_{173}$.

correspond to the shear planes in the model, which have a calculated spacing of 16.4 Å. The calculated inclinations to the coherent boundaries, 54° 52′ in B and 56° 38′ in C, also are close to the observed angles of 56 and 58°, respectively. The model represents the area in Fig. 2a enclosed by the small rectangle. In this case, it should be noted that the black lines drawn on the model correspond to white fringes in the micrograph.

Examples of boundaries between $WNb_{40}O_{103}$ and $WNb_{68}O_{173}$ are shown in Fig. 3a, and a model of the area enclosed by the rectangle is given in Fig. 3b. The Region C in Fig. 3a is $WNb_{40}O_{103}$ and D is $WNb_{68}O_{173}$, the calculated long axis spacings of 26.5 and 44.6 Å, respectively, being in good agreement with the observed spacings of 27 and 45 Å.

The second set of fringes may be identified with the lines running parallel to the rows of blocks in the model. These spacings, 20 Å, and their inclination to the long axis fringes (87° in C, 78° in D) agree reasonably well with calculated values (19.3 Å, 85° 51′ in C, 76° 8′ in D).

The shear plane fringes appear again in Fig. 3 with a spacing of 17 Å (calculated 16.4 Å), inclined to the long axis fringes at 55° in C and 58° in D (calculated inclinations are 56° 38′ and 58° 4′, respectively). In this case the contrast in the micrograph is such

TABLE I

OBSERVED AND CALCULATED UNIT CELL DIMENSIONS

Compound	Pattern in Fig. 1	Cell dimensions (Å)						Symmetry[a]
		Observed			Calculated			
		a	*c*	*β*	*a*	*c*	*β*	
$WNb_{12}O_{33}$[b]	(a)	22.4	19.4	130°	22.0	19.4	130.2°	C
$WNb_{26}O_{68}$	(b)	34.9	19.0	99°	35.3	19.4	98.4°	P
$WNb_{40}O_{103}$	(c)	52.9	19.4	94°	53.1	19.4	93.2°	C
$WNb_{68}O_{173}$	(d)	91.7	19.1	102°	90.8	19.4	100.7°	C
H–Nb_2O_5	(e)	21.2	19.4	120°	20.8	19.4	119.7°	P

[a] C—side-centered monoclinic; P—primitive monoclinic.
[b] The unit-cell setting differs from the one given in Ref. (*2*).

TABLE II

ORDERED INTERGROWTHS OF $WNb_{12}O_{33}$ (A) AND H–Nb_2O_5 (AB)

Ratio B/A	0	1/3	1/2	2/3	1
Combination	A	A_3B	A_2B	A_3B_2	AB
Row sequence[a]	{A, A, A}A	A{B, A, A, A, B}A	A{B, A, A, B, A, A, B}A	A{B, A, A, B, A, A, B, A}A	{A, B, A}B
Composition	$M_{13}O_{33}$	$M_{27}O_{68}$	$M_{41}O_{103}$	$M_{69}O_{173}$	$M_{14}O_{35}$
Symmetry[b]	C	P	C	C	P
Compound	$WNb_{12}O_{33}$	$WNb_{26}O_{68}$	$WNb_{40}O_{103}$	$WNb_{68}O_{173}$	H–Nb_2O_5

[a] The braces give the repeat extension of the rows.
[b] C = side centered; P = primitive.

that black fringes correspond with black lines in the model.

The spacings of sets of fringes and their deviations as they cross coherent phase boundaries are all consistent with the models, and the lattice images are thus able to provide quite detailed confirmation of the proposed structures of these phases and the relationships between them.

Faults and Other Intergrowths

Although we have not specifically looked for faults in these phases, the most common types which occur are a consequence of the disordered intergrowth of the two types of Rows, A and B. There are no cases of the intersecting faults found in other members of the Nb/W series of oxides (*9*), and the

observations in the electron microscope can all be interpreted as the regular or irregular sequence of just these two structural units, representing either a number of finite phase regions, or the intergrowth between them.

Typical faulting is found in both Figs. 2a and 3a. The Fault F in Fig. 2 is evidence for a planar layer of $WNb_{26}O_{68}$, one unit cell wide, which is present in a matrix of $WNb_{40}O_{103}$ (Region C). The spacings between the white fringes in Fig. 2a are all either 27 or 35 Å, and the faulted regions are therefore disordered intergrowths of $WNb_{40}O_{103}$ and $WNb_{26}O_{68}$. A narrow ordered region, marked X in Fig. 2a might be considered to be a microdomain of a new phase, in which half a unit cell of $WNb_{40}O_{103}$ alternates with a unit cell of $WNb_{26}O_{68}$ to give a characteristic new sequence:

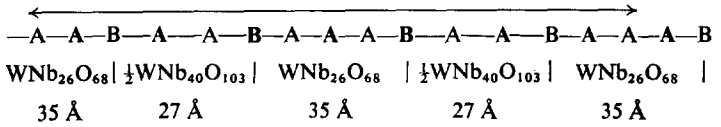

The unit cell, with its extension shown by the arrows, is side-centered, and its dimensions could readily be obtained from a drawing of the idealized model. Since the unit cell contains ten rows of A interspersed with four of B, the composition is

$$10(M_{13}O_{33}) + 4(M_{15}O_{37}) = 2(M_{95}O_{239})$$

corresponding to the compound $W_3Nb_{92}O_{239}$.

A similar ordered Region Y is marked in Fig. 3a, the components in this case being half unit cells of $WNb_{40}O_{103}$ and $WNb_{68}O_{173}$ interleaved with each other. The row sequence is given by

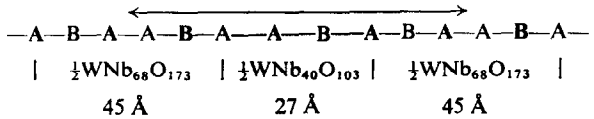

The unit cell, marked by the arrows, is primitive and contains five A and three B Rows. The composition of this domain will be $M_{55}O_{138}$ or $WNb_{54}O_{138}$.

Discussion

The compounds in Nb_2O_5–WO_3 described in Parts I–V of this series of papers (*1–5*) were all found in the first instance by a combination of phase equilibria and X-ray diffraction studies, but none of the three new compounds listed in Table I of the present article has been prepared in pure enough form, or sufficiently well crystallized to be defined by this straightforward approach. Lattice images, on the other hand, are able to amplify the picture in considerably more detail both by locating areas of new phases in preparations, and by providing direct evidence of the most persuasive kind for the defects associated with the phases. These faults may be readily interpreted in terms of exact crystal models when the crystal structures of the phases have been established (*9*) (Part VI). But at the same time the electron microscope studies pose a number of substantial problems of importance to solid state chemistry.

If a single Row B is inserted into a matrix of A, which it can do because of the exact atomic fit between the two at their borders, the structure is unaltered except in its neighborhood,

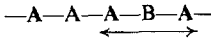

The whole sequence of A can therefore be said to have a single planar fault, but the region marked by the arrow is nevertheless one unit cell of a second phase with the composition (A + B).

Two B Rows can appear in a wide variety of ways, four of which are:

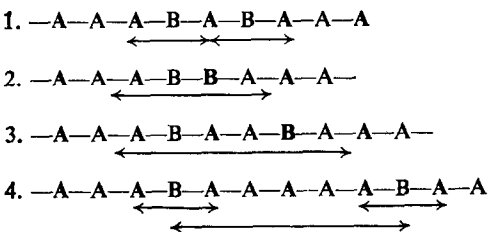

The two units in 1 are associated as two unit cells of the compound with the composition A + B. Much longer sequences of A and B are required to define a unit cell in Examples 2 and 3. But in 4 a decision must be made between two alternatives, whether two unit cells of the compound represented by —A—B—A— appear haphazardly, or whether they are a single unit cell of a phase with a longer repeating sequence.

It is only when there are *several* regularly spaced B

rows giving a unique and well-defined fringe system that clarification of the phase relationships is possible. This is the situation covered by Figs. 2a and 3a which we have used in this account as evidence for the three new compounds $WNb_{68}O_{173}$, $WNb_{40}O_{103}$ and $WNb_{26}O_{68}$, while we have been less decisive about two smaller Regions X and Y identifiable as $W_3Nb_{92}O_{239}$ and $WNb_{54}O_{138}$. Nevertheless no distinction except in size can be made between a single fault and a part of the crystal where a number of the faults constitute a second phase, either by being grouped together, or by forming one of a number of complex sequences with rows of a different kind from the host matrix.

It would certainly be controversial, and yet it may be true, to say that there are few subsolidus phase diagrams dealing with the oxides or chalcogenides of the transition metals that can be regarded as satisfactorily completed. If a compound is "non-stoichiometric," it can exist as a single phase over a composition range. For the niobium–tungsten oxides a single planar fault will reflect a change in the composition of a compound, yet it cannot be expected to alter the X-ray diffraction data, whether recorded as powder or single crystal patterns. Within a crystal an ordered region of a second phase containing just a few unit cells will give the host compound a substantially larger departure from its ideal composition, but will certainly be overlooked even in the most careful X-ray study because the diffracted radiation will be too weak or diffuse to be recorded. This same region, however, can give its characteristic electron diffraction pattern, and will certainly appear in a lattice image provided the crystal is correctly oriented. Because of their shorter wavelengths and the possibility of observing images, the sensitivity of a phase analysis in solid state chemistry is much greater for electrons than it is for X-rays, and defining a nonstoichiometric compound by diffraction methods becomes increasingly inconclusive. Whether or not these classes of compound should be treated as single or multiple phase systems, their apparent homogeneity ranges will depend upon the wavelengths of the radiation used to study them (*10*). Less sensitive methods of defining composition limits overlook the complexity of these and similar systems.

A compound can be expected to form as a unique phase only when its ideal stoichiometry can be guaranteed, and when the reaction to form it is completed. Otherwise the failure of the system to reach an equilibrium state will be reflected in the structure, which in the present instance is evaluated by lattice images.

Ideally this technique should be a powerful and general method for resolving the structural reasons for superlattice formation in solids, but in practice may be limited by their crystal morphology. The growth axes of the block-based niobium–tungsten oxides are parallel to the infinite extension of the blocks, with a common periodicity of 3.8 Å. Being brittle the crushed crystals are searched for a fracture edge, and these are tilted to align the electron beam parallel to this axis. The superstructures of the phases are essentially two-dimensional and in this orientation the diffraction patterns, whether from X-rays or electrons, contain enough information to determine their origin. The sub-cell is derived from the blocks of octahedra having the ReO_3-structure, while the superlattice is contributed by the boundaries between them, the shear planes, which ideally are ordered in a particular way for any one phase. The lattice images may then be generated by one or more of the reciprocal lattice vectors normal to the shear planes, and provide the evidence for faults and for two phase regions.

This technique could not be expected to succeed for layer structures, as platy or micaceous crystals will be oriented flat on the microscope grids. In these circumstances superlattices mainly arise from complex stacking sequences, which will not be revealed until the crystals are reoriented through 90°. The barium ferrites are examples of this class, and are amply documented by the recent X-ray diffraction studies of Kohn and Eckart (*13*, *14*). But in this particular system the electron microscope also has an important role. Cook (*15*) has demonstrated that larger sequences of the most complex kind can be evaluated from replicas of etched basal surfaces exhibiting steps with heights of sub-unit-cell dimensions, which can be identified as structural blocks of two kinds. Defects, which are overlooked in the X-ray case, can also be directly seen and interpreted by this technique, and are usually limited to a few unit cells. The etch method complements the lattice image technique, and both will prove to be powerful tools in the study of solids and of the defects associated with them.

Acknowledgment

We are grateful to Dr. J. V. Sanders for a number of helpful discussions.

References

1. R. S. Roth and A. D. Wadsley, *Acta Cryst.* **19**, 26 (1965).
2. R. S. Roth and A. D. Wadsley, *Acta Cryst.* **19**, 32 (1965).
3. R. S. Roth and A. D. Wadsley, *Acta Cryst.* **19**, 38 (1965).
4. R. S. Roth and A. D. Wadsley, *Acta Cryst.* **19**, 42 (1965).

5. S. ANDERSSON, W. G. MUMME, AND A. D. WADSLEY, *Acta Cryst.* **21**, 802 (1966).
6. R. GRUEHN, *Monatsh. Chem.* **96**, 1789 (1965).
7. R. S. ROTH AND J. L. WARING, *J. Res. Nat. Bur. Standards (Washington)* **70A**, 281 (1966).
8. J. G. ALLPRESS, J. V. SANDERS, AND A. D. WADSLEY, *Phys. Stat. Sol.* **25**, 541 (1968).
9. J. G. ALLPRESS, J. V. SANDERS, AND A. D. WADSLEY, *Acta Cryst.* (in press) (1969).
10. A. D. WADSLEY AND S. ANDERSSON, *in* "Perspectives in Structural Chemistry" (J. D. Dunitz and J. A. Ibers, eds.), Vol. III (in press). Wiley, New York (1969).
11. A. D. WADSLEY, *Acta Cryst.* **14**, 664 (1961).
12. M. LUNDBERG, *Acta Chem. Scand.* (in press) 1969.
13. J. A. KOHN AND D. W. ECKART, *Z. Krist.* **119**, 454 (1964).
14. J. A. KOHN AND D. W. ECKART, *Z. Krist.* **125**, 130 (1967).
15. C. F. COOK, *J. Appl. Physics* **38**, 2488 (1967).